Dalton Transactions

Pushing steric limits in osmium(IV) tetraaryl complexes

Journal:	*Dalton Transactions*
Manuscript ID	DT-ART-06-2022-001706.R1
Article Type:	Paper
Date Submitted by the Author:	20-Jun-2022
Complete List of Authors:	Parr, Joseph; University of Southern California Olivar, Clarissa; University of Southern California Saal, Thomas; University of Southern California, Chemistry; University of Southern California Loker Hydrocarbon Research Institute, Haiges, Ralf; University of Southern California, Chemistry Inkpen , Michael ; University of Southern California,

Pushing steric limits in osmium(IV) tetraaryl complexes

Joseph M. Parr,[a] Clarissa Olivar,[a] Thomas Saal, Ralf Haiges, and Michael S. Inkpen*

Department of Chemistry, University of Southern California, Los Angeles, California 90089, United States

[a] J.M.P. and C.O. contributed equally to this work.

Email: inkpen@usc.edu

ABSTRACT

Investigations into the reactivity, properties, and applications of osmium(IV) tetraaryl complexes have been hampered by their low yielding syntheses from volatile and toxic OsO_4 (typically ≤34%). Here we show that known air-stable $M(aryl)_4$ compounds (M = Os, Ru; aryl = 2-tolyl, 2,5-xylyl) can be prepared in ≤73% yields using new, less hazardous $(Oct_4N)_2[MX_6]$ precursors (M = Os, Ru; X = Cl, Br). This approach also facilitates the preparation of $Os(mesityl)_4$ (**Os3**) for the first time, a complex comprising bulky 2,6-dimethyl substituted aryl ligands, albeit in low yield (5%). To better understand these yield extremes, we track, by synthesizing two additional new complexes with different 2-substituted σ-aryl ligands, a clear relationship between the yields of $Os(aryl)_4$ and ligand steric bulk. Single-crystal X-ray structures of these compounds indicate that the observed yield trend reflects the ease of accommodating aryl substituents into an open pocket that lies directly opposite each M-aryl coordination site. We perform variable-temperature ^{1}H NMR studies of **Os3**, utilize a "tetrahedricity" metric to assess geometric distortion in $Ru(aryl)_4$ and $Os(aryl)_4$ materials, and calculate cone angle and percentage buried volume metrics to further illustrate and help quantify *σ*-aryl ligand steric properties. Solution cyclic voltammograms of $Os(aryl)_4$ show that the potentials of their reversible 1−/0 and 0/1+ redox features can be fine-tuned by varying aryl substituents, and that **Os3** exhibits an additional 1+/2+ redox event not previously observed in this class of compounds. Taken together, this work helps to advance the potential application of these relatively underexplored organometallic complexes in established and emerging areas of molecular materials science, such as extended molecular frameworks and self-assembled monolayers, where analogous tetraphenylmethane and silane species (M = C, Si) have been frequently targeted.

INTRODUCTION

Homoleptic transition metal(IV) tetraaryl complexes, $M(aryl)_4$, are an underexplored class of organometallic materials with distinct electrochemical, magnetic, and optical characteristics resulting from their tetrahedral coordination geometry.[1] Their properties complement and extend beyond those of their isostructural group 14 congeners, widely utilized as primary components of advanced molecular materials such as covalent- and metal-organic frameworks,[2–5] polymers,[6] self-assembled monolayers,[7–10] and single-molecule electronic components.[11,12] We anticipate that modular, isostructural $M(aryl)_4$ units can provide new approaches, for example, to tune the electrochemical energy storage capacity, electrocatalytic function, and electrical conductivity/conductance of such materials, among other applications. Notable in this context, $Cr(aryl)_4$ complexes have recently been shown to function as optically accessible molecular qubits for quantum information applications after spatial isolation through dispersion in a $Sn(aryl)_4$ diluent matrix.[13,14]

Among the reported $M(aryl)_4$ materials, Os(IV)[15–17] and Ru(IV)[16–18] compounds with ortho-methylated σ-aryl ligands are particularly robust. As stated by Wilkinson *et al.* their stability is consistent with a d^4 low-spin electronic configuration, with the ligand methyl groups serving to inhibit decomposition pathways including reductive elimination and *ortho*-hydrogen abstraction.[16] These compounds can be purified using chromatography in air, and their aryl ligands can be chemically functionalized via different methods (including bromination,[19] Suzuki coupling,[19] and Friedel-Crafts acylation[20]). $Os(aryl)_4$ also have a particularly rich redox chemistry which facilitated the early isolation of a stable paramagnetic Os(V) complex.[21] However, $Os(aryl)_4$ are often obtained in poor yields (typically ≤34%, see **SI, Table S2**) from reactions of aryl Grignard reagents with OsO_4 (**Figure 1**, top; aryl = 2-tolyl, 2,5-xylyl, 2,4-xylyl, 4-fluoro-2-tolyl, and phenyl). Given the high toxicity of OsO_4, and additional purification complications caused by the presence of monooxo(tetraaryl)osmium(VI)[22] and bisoxo(diaryl)osmium(VI)[22,23] side products, the development of higher-yielding preparative approaches using alternative starting reagents is desirable.

In this work we report an improved synthetic route to osmium(IV) tetraaryl complexes starting from new tetra-*n*-octylammonium hexahaloosmate(IV) precursors $(Oct_4N)_2[OsX_6]$ (X = Cl, Br; route with X = Br shown in **Figure 1**, bottom); this approach can also be used to prepare ruthenium homologues from tetra-*n*-octylammonium hexachlororuthenate(IV), $(Oct_4N)_2[RuCl_6]$. Reactions of the appropriate aryl Grignard reagent with $(Oct_4N)_2[OsBr_6]$ provide Os(2-tolyl)$_4$ (**Os1**) and Os(2,5-xylyl)$_4$ (**Os2**) in among the highest yields reported for any $M(aryl)_4$ compound prepared to date (55-73%). From reactions with mesitylmagnesium

bromide we obtain Os(mesityl)$_4$ (**Os3**) in 5% isolated yield, a previously inaccessible complex comprising sterically demanding 2,6-dimethyl substituted aryl ligands. In applying analogous methods to synthesize Os(2-ethylphenyl)$_4$ (**Os1-Et**, obtained in 41% yield) and Os(2-*iso*-propylphenyl)$_4$ (**Os1-*i*Pr**, 14% yield), we observe a clear correlation between the efficiency of Os(aryl)$_4$ formation and ligand steric bulk. We further rationalize this trend by comparing the molecular structures of **Os1-3**, **Os1-Et**, and **Os1-*i*Pr** obtained from single-crystal X-ray diffraction studies (**Figure 2**), using quantitative metrics for coordination geometry distortion and for σ-aryl ligand steric properties (e.g., **Figure 3**), and explore how the redox properties of differently substituted Os(aryl)$_4$ vary using solution electrochemistry (**Figure 5**).

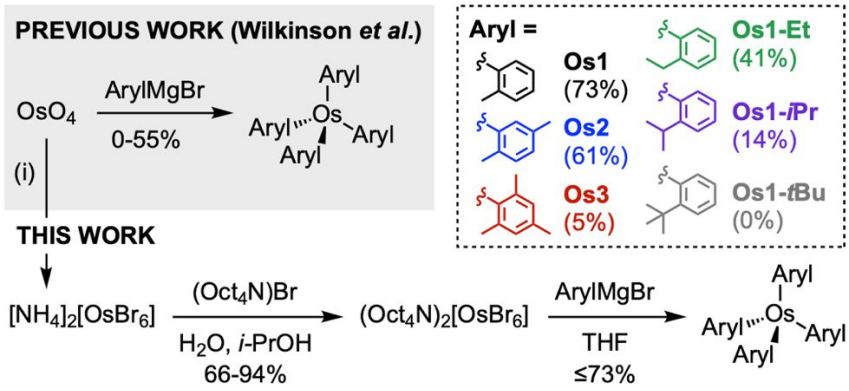

Figure 1. Synthetic routes to Os(aryl)$_4$ complexes from reactions of aryl Grignard reagents with OsO_4 (previous work, top) or $(Oct_4N)_2[OsBr_6]$ (this work, bottom); (i) = HBr, NH_4Br, ethanol.[24] Use of $(Oct_4N)_2[OsBr_6]$ mitigates the formation of osmium(VI) oxoaryl side products, provides higher yields of Os(aryl)$_4$, and facilitates the formation of Os(mesityl)$_4$ (**Os3**) for the first time. Inset, yields of complexes decrease with increasing steric bulk of the σ-aryl ligand.

EXPERIMENTAL SECTION

Materials and Instruments

All manipulations were carried out in oven-dried glassware under a nitrogen atmosphere using standard Schlenk line techniques. No special precautions were taken to exclude air or moisture during workup unless otherwise stated. Tetrahydrofuran and dichloromethane were sparged with nitrogen and dried using a two-column solvent purification system packed with alumina (Pure Process Technologies, Nashua, NH, USA). Grignard reagents were commercially available, or prepared according to the general method described here, and titrated using a salicylaldehyde phenylhydrazone indicator to determine their concentration prior to use.[25] Additional notes on Grignard preparation can be found in the supporting information. Flash

chromatography was performed using a Pure C-850 FlashPrep chromatography system and FlashPure EcoFlex flash cartridges (silica, irregular 40-63 μm particle size, 55-75 Å pore size; BUCHI Corporation, New Castle, DE, USA), or manually using Alfa Aesar silica gel 60 (215-400 mesh). $(Oct_4N)_2[RuCl_6]$[26] was prepared using established literature procedures. $(NH_4)_2[OsCl_6]$[27] and $(NH_4)_2[OsBr_6]$[28] were prepared using established literature procedures or purchased from commercial suppliers. All other chemical reagents were commercially available and used without further purification.

^1H and $^{13}C\{^1H\}$ NMR spectra were recorded at room temperature on Varian VNMRS 500 (500 MHz), 400MR (400 MHz), VNMRS 600 (600 MHz), or Mercury 400 (400 MHz) NMR spectrometers, unless otherwise stated. ^1H NMR data recorded in $CDCl_3$, CD_2Cl_2, C_6D_6, and toluene-d_8 is referenced to residual internal C*H*Cl_3 (δ 7.26), CD*H*Cl_2 (δ 5.32), C_6D_5H (δ 7.16), and $C_6D_5CD_2H$ (δ 2.08) solvent signals.[29] $^{13}C\{^1H\}$ NMR data recorded in $CDCl_3$ is referenced to internal *C*DCl_3 (δ 77.16).[29] ^1H and $^{13}C\{^1H\}$ resonances were assigned where possible using 2D correlation spectroscopy experiments. Variable-temperature NMR measurements were performed on a Varian VNMRS 600 (600 MHz) NMR spectrometer, with temperatures calibrated using a 4% CH_3OH in CD_3OD sample containing a trace of HCl.[30] Infrared spectra were obtained using an Agilent compact Cary 630 FTIR spectrometer fitted with a diamond ATR sampling module and KBr window. Mass spectrometry analyses were performed on an Agilent 6545 QTOF mass spectrometer fitted with an atmospheric pressure electrospray ionization source (Dual AJS ESI) at the University of Southern California (USC), or on a Waters Synapt G2-Si (ESI) or Waters GCT Premier (EI) at the Mass Spectrometry Lab, University of Illinois Urbana-Champaign. Microanalyses were carried out using a Thermo Flash 2000 CHNS Combustion Analyzer at USC, or on a Control Equipment Corp. CEC 440HA Elemental Analyzer at the Marine Science Institute, University of California Santa Barbara. Electrochemical measurements were performed under an argon atmosphere using a CHI760E bipotentiostat (CH Instruments, Austin, TX, USA) with anhydrous, nitrogen-sparged 0.1 M tetrabutylammonium hexafluorophosphate (NBu_4PF_6) dichloromethane solutions. We used a glassy carbon disc working electrode (Ø = 3 mm, CH Instruments), with Pt wire reference and counter electrodes. Glassy carbon electrodes were mechanically polished using an alumina slurry prior to use, Pt wires were cleaned by annealing in an oxyhydrogen flame. Analyte solutions were between 0.1-1 mM. Potentials are reported relative to $[Cp_2Fe]^+/[Cp_2Fe]$, measured against internal Cp_2Fe or Cp^*_2Fe references as appropriate.

$(Oct_4N)_2[OsCl_6]$

This method is adapted from the synthesis of $(Oct_4N)_2[RuCl_6]$.[26] A solution of tetra-*n*-octylammonium bromide (1.470 g, 2.69 mmol) in 2-propanol (50 mL) was added to an aqueous solution of $(NH_4)_2[OsCl_6]$ (0.577 g, 1.31 mmol) in deionized water (45 mL). After stirring for 1 h, deionized water (10 mL) was added and the precipitate collected via filtration in air. This was rinsed with deionized water (3 x ~20 mL) and dried under vacuum overnight to provide a yellow powder (1.521 g, 87% yield). ^{1}H NMR ($CDCl_3$, 500 MHz): δ (ppm) 0.87 (t, 12H, J = 6.8 Hz), 1.21-1.33 (m, 24H), 1.37 (m, 8H), 1.49 (m, 8H), 1.77 (m, 8H), 3.23 (m, 8H).^{13}C{^{1}H} NMR ($CDCl_3$, 125 MHz): δ (ppm) 13.83, 22.38, 24.30, 27.56, 28.88, 29.38, 31.52, 69.04. Anal. Calc. for $C_{64}H_{136}N_2Cl_6Os$: C, 57.59; N, 2.10; H, 10.27%. Found: C, 57.64; N, 2.04; H, 10.22%.

$(Oct_4N)_2[OsBr_6]$

This representative procedure is adapted from the synthesis of $(Oct_4N)_2[RuCl_6]$.[26] Deionized water (46 mL) and 2-propanol (26 mL) were added to a flask containing tetra-*n*-octylammonium bromide (1.6783 g, 3.07 mmol) and $(NH_4)_2[OsBr_6]$ (1.085 g, 1.54 mmol). The mixture was stirred for 1 h at room temperature. The red oil/solid that precipitated was separated from the filtrate, and then extracted into CH_2Cl_2/H_2O. The combined organic phases provided a red solid after solvent evaporation which was redissolved in CH_2Cl_2, and the solution filtered through a plug of sand. The red-brown solid obtained after removal of solvent was dried under vacuum to afford the analytically pure product (2.3028 g, 94%). Repeated syntheses show yields can vary but are always ≥66%. If necessary, the product can be further purified by extensive washing with deionized water and 2-propanol, or recrystallization from CH_2Cl_2/2-propanol. ^{1}H NMR ($CDCl_3$, 500 MHz): δ (ppm) 0.87 (t, 12H, J = 5.7 Hz), 1.22-1.35 (m, 24H), 1.39 (m, 8H), 1.50 (m, 8H), 1.77 (m, 8H), 3.22 (m, 8H). ^{13}C{^{1}H} NMR ($CDCl_3$, 125 MHz): δ (ppm) 13.38, 21.92, 24.40, 27.76, 28.45, 29.08, 31.09, 69.70. HR-MS (ESI) *m/z*: 466.5352 ($[Oct_4N]^+$ calc. for $C_{32}H_{68}N$: 466.5352), 590.5464 ($[OsBr_5]^-$ calc. for $OsBr_5$: 590.5491). Anal. Calc. for $C_{64}H_{136}N_2Br_6Os$: C, 47.94; N, 1.75; H, 8.55%. Found: C, 48.30; N, 1.85; H, 8.69% (average of two runs).

General Synthesis of M(aryl)$_4$ Complexes from $(Oct_4N)_2[MX_6]$ (M = Os, Ru; X = Cl, Br)

A solution of the appropriate aryl Grignard reagent in THF was added dropwise to a stirred suspension of $(Oct_4N)_2[MX_6]$ in THF. The mixture was stirred at room temperature for 2 h, then nitrogen-sparged methanol (1 mL) was added. The solvent was removed *in vacuo*. The resulting solid was dissolved in CH_2Cl_2, packed onto Celite and purified by automated flash chromatography in air (silica; hexanes/CH_2Cl_2, 1:0→4:1).

*Os(2-tolyl)$_4$ (**Os1**)*

From $(Oct_4N)_2[OsCl_6]$: 2-Tolylmagnesium bromide in THF (0.66 mL, 0.9 M, 0.60 mmol), $(Oct_4N)_2[OsCl_6]$ (0.113 g, 0.085 mmol), and THF (10 mL) provided a black solid (0.014 g, 30%). From $(Oct_4N)_2[OsBr_6]$: 2-Tolylmagnesium bromide in THF (2.40 mL, 0.9 M, 2.16 mmol), $(Oct_4N)_2[OsBr_6]$ (0.494 g, 0.31 mmol), and THF (10 mL) provided a black solid (0.124 g, 73%). Spectroscopic data were consistent with previous reports.[16,31] ^{1}H NMR ($CDCl_3$, 400 MHz): δ (ppm) 2.30 (s, 12H, -C*H*$_3$), 6.79 (m, 8H, aryl-*H*), 6.94 (m, 8H, aryl-*H*). ^{1}H NMR (toluene-d_8, 400 MHz): δ (ppm) 2.30 (s, 12H, -C*H*$_3$), 6.60 (m, 8H, aryl-*H*), 6.78 (m, 4H, aryl-*H*), 7.04 (d, 4H, aryl-*H*). ^{1}H NMR (benzene-d_6, 400 MHz): δ (ppm) 2.34 (s, 12H, -C*H*$_3$), 6.64 (m, 8H, aryl-*H*), 6.81 (m, 4H, aryl-*H*), 7.09 (d, 4H, aryl-*H*). ^{13}C{^{1}H} NMR ($CDCl_3$, 125 MHz): δ (ppm) 25.73 (-*C*H$_3$), 124.44 (aryl, *C*H), 127.95 (aryl, *C*H), 128.14 (aryl, *C*H), 135.05 (aryl, *C*H), 137.66, 140.57. HR-MS (EI) *m/z*: 556.1805 ([M]$^+$ calc. for $C_{28}H_{28}Os$: 556.1806).

*Os(2,5-xylyl)$_4$ (**Os2**)*

From $(Oct_4N)_2[OsCl_6]$: 2,5-Xylylmagnesium bromide in THF (0.55 mL, 1.04 M, 0.57 mmol), $(Oct_4N)_2[OsCl_6]$ (0.108 g, 0.08 mmol), and THF (10 mL) afforded a black powder (0.020 g, 40%). From $(Oct_4N)_2[OsBr_6]$: **(A)** 2,5-Xylylmagnesium bromide in THF (2.5 mL, 0.53 M, 1.33 mmol), $(Oct_4N)_2[OsBr_6]$ (0.293 g, 0.18 mmol), and THF (4 mL) provided a black powder (0.069 g, 61%). **(B)** 2,5-Xylylmagnesium bromide in THF (24.77 mL, 0.87 M, 21.55 mmol), $(Oct_4N)_2[OsBr_6]$ (4.921 g, 3.07 mmol), and THF (100 mL) afforded a black powder (1.032 g, 55%). From OsO_4: A solution of 2,5-xylylmagnesium bromide in THF (14 ml, 0.5 M, 7 mmol) was added dropwise to a stirred suspension of OsO_4 (0.250g, 0.98 mmol) in THF (10 ml) at −78°C under nitrogen. The resulting reddish-brown mixture was allowed to warm to room temperature and stirred for 2 h, then nitrogen-sparged methanol (1 mL) was added. The solvent was removed *in vacuo* to provide the crude product. This was found by ^{1}H NMR to consist of a mixture of **Os2** and OsO(2,5-xylyl)$_4$[22] in an approximate 2:1 ratio. The resulting crude material was dissolved in hexanes, packed onto Celite and purified by automated flash chromatography in air (silica; hexanes/diethyl ether, 1:0→99:1) to provide **Os2** as a black solid (0.039 g, 6%). The low isolated yield is due to challenging separation from the closely eluting OsO(2,5-xylyl)$_4$[22] species.

Crystals suitable for X-ray diffraction were grown by cooling a solution of **Os2** in *n*-hexane to −20°C (red-brown plate-like crystals). Spectroscopic data were consistent with previous reports.[19,22] ^{1}H NMR ($CDCl_3$, 500 MHz): δ (ppm) 2.24 (s, 12H, 5-C*H*$_3$), 2.28 (s, 12H, 2-C*H*$_3$), 6.59 (d, 4H, *J* = 7.5 Hz, 4-C*H*), 6.69 (d, 4H, *J* = 7.5 Hz, 3-C*H*), 6.72 (s, 4H, 6-C*H*).

$^{13}C\{^1H\}$ NMR ($CDCl_3$, 150 MHz): δ (ppm) 21.24 (5-*C*H_3), 25.34 (2-*C*H_3), 127.44 (aryl, 3-*C*H), 128.73 (aryl, 4-CH), 133.60 (aryl, *C*-Os), 135.11 (aryl, 6-*C*H), 137.32 (aryl, 2-*C*Me), 138.12 (aryl, 5-*C*Me). HR-MS (ESI/Q-TOF) *m/z*: 612.2433 ($[M]^+$ calc. for $C_{32}H_{36}Os$: 612.2432).

*Os(mesityl)$_4$ (**Os3**)* and *OsO$_2$(mesityl)$_2$*

Mesitylmagnesium bromide in THF (2.88 mL, 0.94 M, 2.71 mmol), $(Oct_4N)_2[OsBr_6]$ (0.618 g, 0.39 mmol), and THF (10 mL) provided **Os3** (0.014 g, 5%) as a green-black solid from selected fractions of the black band eluting with hexanes/CH_2Cl_2 (9:1). Crystals suitable for X-ray diffraction were grown by cooling a solution in *n*-hexane to −20°C (green-black needles). ^1H NMR ($CDCl_3$, 500 MHz): δ (ppm) 2.11 (br s, 24H, 2,6-C*H*$_3$), 2.36 (s, 12H, 4-C*H*$_3$), 6.47 (br s, 8H, 3,5-C*H*). $^{13}C\{^1H\}$ NMR ($CDCl_3$, 100 MHz): δ (ppm) 20.20, 126.23, 127.64, 138.10 (only 4 of 6 expected resonances observed). HR-MS (ESI/Q-TOF) *m/z*: 668.3066 ($[M]^+$ calc. for $C_{36}H_{44}Os$: 668.3058). $OsO_2(mesityl)_2$ was obtained as a green solid from fractions of the green band eluting with hexanes/CH_2Cl_2 (4:1) (0.022 g, 12%). Crystals suitable for X-ray diffraction were grown by slow evaporation of a *n*-hexane/CH_2Cl_2 solution (dark green needles). Spectroscopic data were consistent with previous reports.[23] ^1H NMR ($CDCl_3$, 500 MHz): δ (ppm) 2.34 (s, 12H, 2,6-C*H*$_3$), 2.54 (s, 6H, 4-C*H*$_3$), 7.00 (s, 4H, 3,5-C*H*). ^1H NMR (C_6D_6, 400 MHz): δ (ppm) 2.27 (s, 6H, 4-C*H*$_3$), 2.35 (s, 12H, 2,6-C*H*$_3$), 6.74 (s, 4H, 3,5-C*H*). IR (ATR): *v* (cm^{-1}) 950, 917 (Os=O).

*Os(2-ethylphenyl)$_4$ (**Os1-Et**)*

2-Ethylphenylmagnesium bromide in THF (3.4 mL, 0.47 M, 1.60 mmol), $(Oct_4N)_2[OsBr_6]$ (0.306 g, 0.19 mmol), and THF (7 mL) provided a black solid (0.047 g, 41%). ^1H NMR ($CDCl_3$, 600 MHz): δ (ppm) 0.52 (t, 12H, *J* = 7.38 Hz, -C*H*$_3$), 2.48 (br s, 8H, -C*H*$_2$-), 6.80 (m, 4H, aryl-*H*), 6.92 (m, 12H, aryl-*H*). $^{13}C\{^1H\}$ NMR ($CDCl_3$, 150 MHz): δ (ppm) 15.58 (-*C*H_3), 32.63 (-*C*H_2-), 125.18 (aryl, *C*H), 126.12 (aryl, *C*H), 127.99 (aryl, *C*H), 134.93 (aryl, *C*-Os), 137.00 (aryl, *C*H), 147.52 (aryl, *C*Et). HR-MS (ESI/Q-TOF) *m/z*: 612.2454 ($[M]^+$ calc. for $C_{32}H_{36}Os$: 612.2432).

*Os(2-*iso*-propylphenyl)$_4$ (**Os1-iPr**)*

2-*Iso*-propylphenylmagnesium bromide in THF (2.6 mL, 0.58 M, 1.51 mmol), $(Oct_4N)_2[OsBr_6]$ (0.300 g, 0.19 mmol), and THF (5 mL) provided a black powder (0.0171 g, 14%). ^1H NMR ($CDCl_3$, 600 MHz): δ (ppm) 0.22 (d, 12H, *J* = 6.6 Hz, -C*H*$_3$), 1.22 (d, 12H, *J* = 6.6 Hz, -C*H*$_3$), 2.51 (sept, *J* = 6.48 Hz, 4H, -C*H*$(CH_3)_3$), 6.82 (t, *J* = 5.76 Hz, 4H, aryl-H),

6.95 (m, 12H, aryl-H).$^{13}C\{^1H\}$ NMR ($CDCl_3$, 150 MHz): δ (ppm) 24.21 (-*C*H_3), 24.54 (-*C*H_3), 37.19 (-*C*H(CH_3)$_2$), 123.17 (aryl, 3-*C*H), 125.49 (aryl, *C*H), 128.12 (aryl, *C*H), 133.99 (aryl, *C*-Os), 138.15 (aryl, *C*H), 152.97 (aryl, *C*-^{i}Pr). HR-MS (ESI/Q-TOF) *m/z*: 668.3072 ($[M]^+$ calc. for $C_{36}H_{44}Os$: 668.3058).

*Ru(2-tolyl)$_4$ (**Ru1**)*

From $(Oct_4N)_2[RuCl_6]$: 2-Tolylmagnesium bromide in THF (4.75 mL, 0.9 M, 4.28 mmol), $(Oct_4N)_2[RuCl_6]$ (0.253 g, 0.20 mmol), and THF (10 mL) yielded a red-brown powder (0.034 g, 36%). Spectroscopic data were consistent with previous reports.[17] ^1H NMR ($CDCl_3$, 600 MHz): δ (ppm) 2.13 (s, 12H, -CH_3), 6.90 (d, 4H, J = 5.8 Hz, aryl-*H*), 7.00 (m, 8H, aryl-*H*), 7.20 (d, 4H, J = 6.2 Hz, aryl-*H*). HR-MS (ESI/Q-TOF) *m/z*: 466.1243 ($[M]^+$ calc. for $C_{28}H_{28}Ru$: 466.1234).

X-Ray Crystallography

X-ray intensity data were collected at 100 K either on a Bruker APEX DUO 3-circle platform diffractometer, equipped with an APEX II CCD detector, or a Rigaku XtaLAB Synergy, Dualflex, equipped with a HyPix-6000HE CCD detector, using MoKα radiation (λ = 0.71073 Å, TRIUMPH curved-crystal monochromator) from a fine-focus tube. The structures were solved by intrinsic phasing and refined on F^2 using the Bruker SHELXTL Software Package and ShelXle.[32–35] All non-hydrogen atoms were refined anisotropically. Further crystallographic details can be obtained from the Cambridge Crystallographic Data Centre (CCDC, 12 Union Road, Cambridge, CB2 1EZ, UK (Fax: (+44) 1223–336–033; e-mail: deposit@ccdc.cam.ac.uk) on quoting the deposition no. CCDC 2024175, 2024176, 2119165, 2175533, 2175534.

Calculation of Ligand Parameters

The geometries and ligand parameters for Os-aryl fragments were obtained as follows, unless otherwise stated. First, the ground state geometries of the uncoordinated, protonated σ-aryl ligands (e.g., toluene for 2-tolyl) were optimized at the B3LYP/6-31G level; with density functional theory (DFT) calculations performed using the Q-Chem 5.2 program through the molecular editor and visualization package IQMol 2.15.[36] The *ipso* H was replaced by an Os atom, and the Os-aryl bond set to 1.997 Å (the average Os-aryl bond length in **Os1**, see **Table 1**). The 2-substituents for each σ-aryl ligand were subsequently rotated about their C-C bonds to provide the minimum *in-plane* cone angle (Θ_{in}) as defined in **Figure 3**. Exported atomic coordinates were plotted as ball and stick models in Mercury 4.3.1 (Cambridge

Crystallographic Data Centre, Cambridge, UK) to determine Θ_{in} and Θ_{out}, or used as an input for the SambVca 2.1 web applet to calculate $\%V_{bur}$.[37] The $\%V_{bur}$ calculations used a sphere radius of 3.5 Å, a mesh spacing for numerical integration of 0.1 Å, and atomic radii corresponding to the unscaled (Bondii) van der Vaals radii, with hydrogen atoms excluded from the calculations.

RESULTS AND DISCUSSION

In developing a new synthetic route to $Os(aryl)_4$, we first considered approaches that might reduce or eliminate the formation of osmium(VI) oxoaryl side products. These are reported to originate from the incomplete substitution of OsO_4 rather than through air oxidation in solution or during chromatographic purification.[22] We reasoned that the formation of such side products could therefore be mitigated by using alternative oxygen-free osmium precursors, and looked for inspiration from the materials used to prepare analogous ruthenium(IV) tetraaryl complexes. These include $(Et_4N)[RuCl_5(THF)]$,[17] $(Et_4N)[RuCl_5(MeCN)]$,[17] $Ru_2(\mu\text{-}O_2CMe)_4$,[17] $RuCl_3(tht)_3$,[18] and $Ru(acac)_3$[38,39] (tht = tetrahydrothiophene, acac = acetylacetonate). Unfortunately, yields of the $Ru(aryl)_4$ products are also low (**SI, Table S1**), and methods involving some of these precursors are reportedly difficult to reproduce.[17,18] We therefore sought alternative easily accessible M(IV) compounds, noting that multinuclear, Ru(II), or Ru(III) species increase the complexity of reactions (potentially involving disproportionation reactions to form Ru(IV)[17]) and that the mononuclear pentachlororuthenate salts[17] have not been utilized since the first synthetic reports of $Ru(aryl)_4$ compounds. Remarkably, several members of the family of $(NH_4)_2[MX_6]$ salts (M = Os, Ru; X = Cl, Br) are commercially available or readily synthesized using verified protocols,[27,28] but have not yet been explored as precursors to $M(aryl)_4$ compounds.

We first evaluated the commercially available, and/or previously reported, $(NR_4)_2[RuCl_6]$ salts (R = H, octyl).[26] Initial attempts to prepare $Ru(2\text{-tolyl})_4$ (**Ru1**) through the addition of 6-8 equivalents of 2-tolylmagnesium bromide to $(NH_4)_2[RuCl_6]$ proved unsuccessful due to the low solubility of the metal salt in THF and diethyl ether (coordinating solvents commonly used for Grignard reactions). Following cation exchange to increase the solubility of the anion in common organic solvents, and to eliminate possible quenching of Grignard reagent with the protic ammonium cations, the analogous reaction using $(Oct_4N)_2[RuCl_6]$[26] provided **Ru1** in 36% yield (**SI, Figure S1**). This yield was comparable to those from previously reported routes using different ruthenium precursors (**SI, Table S1**). We

subsequently adapted this cation exchange protocol to prepare the new organosoluble Os(IV) starting materials $(Oct_4N)_2[OsCl_6]$ and $(Oct_4N)_2[OsBr_6]$ in 87% and 94% yield, respectively (**Figure 1**, bottom). Reactions between $(Oct_4N)_2[OsX_6]$ and the appropriate arylmagnesium bromide provided **Os1** (X = Cl, 30%; X = Br, 73%) and **Os2** (X = Cl, 40%; X = Br, 61%) in among the highest yields for $M(aryl)_4$ reported to date (see **SI, Table S2** for a summary of previous work). Using $(Oct_4N)_2[OsBr_6]$ we find this preparative approach is scalable, facilitating the synthesis of **Os2** in >1 g quantities (55% yield). Notably, **Os1-3** and **Ru1** were all worked up in air and are readily purified by chromatography; we anticipate their chemical stability will prove useful in isolating derivatized or heteroleptic analogues in the future. While previous routes to $M(aryl)_4$ have reported their direct purification through recrystallisation, we note that this approach is inhibited when using $(Oct_4N)_2[MX_6]$ reagents. A viscous crude reaction product is obtained after solvent removal which limits full extraction of reaction products into hexanes. In line with previous reports, however, we find that isolated $M(aryl)_4$ are readily crystallized from solution. It is stressed here that for consistent yields, $(Oct_4N)_2[OsBr_6]$ samples of analytical purity must be used.

The higher yields of $Os(aryl)_4$ obtained when using $(Oct_4N)_2[OsBr_6]$ compared to $(Oct_4N)_2[OsCl_6]$ suggests that the nature of the metal halide plays a critical role in the formation of these complexes. Noting trends observed for related materials, the Os-Br bonds in $(Oct_4N)_2[OsX_6]$ should have lower heterolytic bond energies than Os-Cl.[40,41] We hypothesize that this, in combination with the greater steric crowding around the M(IV) centre in $[OsBr_6]^{2-}$ compared to $[OsCl_6]^{2-}$, increases the rate of loss of the larger bromide ions and subsequent coordination of σ-aryl ligands to the Os centre via a dissociative mechanism. While the focus of this initial study is on $Os(aryl)_4$ complexes, we anticipate that reactions from precursors such as $(Oct_4N)_2[RuBr_6]$ (containing Ru-Br rather than Ru-Cl bonds) would also provide improved yields of $Ru(aryl)_4$ complexes compared to $(Oct_4N)_2[RuCl_6]$.

To test the potential of our new synthetic approach we next targeted the preparation of **Os3**, an otherwise inaccessible bulky 2,6-disubstituted $Os(aryl)_4$ complex. Previous reactions of OsO_4 with mesitylmagnesium bromide resulted only in the isolation of $OsO_2(mes)_2$,[16,23] and with 2,6-xylylmagnesium bromide yielded only $OsO_2(2,6\text{-xylyl})_2$.[42] In contrast here, the reaction of mesitylmagnesium bromide with $(Oct_4N)_2[OsBr_6]$ provided **Os3** as a green-black solid in 5% yield in addition to $OsO_2(mes)_2$ (12%).[23] Though the ^1H and $^{13}C\{^1H\}$ NMR spectra of these two products are somewhat ambiguous, each showing only resonances attributable to mesityl ligands, their identity could be verified through single-crystal X-ray diffraction (**Figure 2** and **SI, Figure S2**) and IR spectroscopy (**SI, Figure S6**). Of all the osmium compounds

described here, only $OsOs_2(mes)_2$ exhibits IR spectral features attributable to Os=O. Given that $(Oct_4N)_2[OsBr_6]$ contains no oxo groups, we propose that $OsO_2(mes)_2$ forms through incomplete substitution of the $[OsBr_6]^{2-}$ ion, followed by hydrolysis/oxygen abstraction during reaction workup in air or during chromatographic purification. $OsO_2(aryl)_2$ species were not readily observed or isolated during analogous reactions with less bulky ligands, but their formation is evidently not precluded under these reaction conditions. We attribute the low yield of **Os3** to the steric constraints of incorporating four 2,6-dimethylated aryl ligands around the Os(IV) centre (see discussion below). Analogous ruthenium complexes comprising bulky ligands are also reported in relatively lower yields; Ru(mesityl)$_4$ and Ru(2,6-xylyl)$_4$ were prepared in 13-21% yield[17] compared to 24-48% for Ru(aryl)$_4$ complexes with a single 2-methyl substituent (**SI, Table S1**). Additional evidence for steric congestion around the osmium centre in **Os3** is provided by its ^{1}H NMR spectrum. This reveals significantly broadened *ortho*-C*H*$_3$ and *meta*-*H* resonances (**SI, Figure S15**), indicative of restricted rotation of the mesityl ligand around the Os-aryl σ-bond at room temperature. Through variable temperature NMR studies, we find that that the Gibbs free energy of activation ($\Delta G^{\ddagger}$) for **Os3** is ~47 kJ mol^{-1}, compared to ~50 kJ mol^{-1} for Ru(mesityl)$_4$ (**Ru3**; see the **SI, Figure S23** and **Table S30**). The similarity between these $\Delta G^{\ddagger}$ is consistent with their comparable bond lengths (within 3 estimated standard deviations, where **Os3**$_{(Os\text{-}C)}$ = 2.037(3) Å, **Ru3**$_{(Ru\text{-}C)}$ = 2.01(1) Å; see discussion below and **Table 1**). For structurally similar complexes, it was previously noted that the longer the M-C bond length the lower the value of $\Delta G^{\ddagger}$.[43]

To further explore the apparent influence of ligand steric effects on yields, we pursued the synthesis of additional Os(aryl)$_4$ comprising different 2-substituents of increasing size: Os(2-ethylphenyl)$_4$ (**Os1-Et**), Os(2-*iso*-propylphenyl)$_4$ (**Os1-*i*Pr**), and Os(2-*tert*-butylphenyl)$_4$ (**Os1-*t*Bu**). From analogous reactions between $(Oct_4N)_2[OsBr_6]$ and the appropriate Grignard reagent, we obtained **Os1-Et** and **Os1-*i*Pr** in 41% and 14% yields, respectively. While the stabilization of Os(aryl)$_4$ complexes has only previously been demonstrated with methyl substituents, other 2-substituents are clearly able to perform this function. However, our attempts to prepare **Os1-*t*Bu** from $(Oct_4N)_2[OsBr_6]$ and 2-*tert*-butylphenyl magnesium bromide under analogous conditions have proved unsuccessful. These results clearly demonstrate that the yields of Os(aryl)$_4$ increase with decreasing ligand steric bulk: 2-*tert*-butylphenyl (no isolable complex) > mes (5%) > 2-*iso*-propylphenyl (14%) > 2-ethylphenyl (41%) > 2,5-xylyl (61%) > tolyl (73%) (**Figure 1**, inset).

To gain further insights into these trends, we obtained the solid-state structures of **Os2**, **Os1-Et**, **Os1-*i*Pr**, and **Os3** by single-crystal X-ray diffraction and compared them to analogous

previously characterized tetrahedral compounds (**Figure 2**, **Table 1** and **SI, Tables S13-S28**). We observe no clear correlation between M-C bond lengths and aryl substituents across the series but recognize that the complexes with more sterically bulky ligands (such as mesityl, cyclohexyl, 2-*iso*-propylphenyl) have longer M-C bond lengths than those with smaller ligands (e.g., tolyl). The range of angles between aryl planes also does not appear to correlate with the number of ortho-substituents or the electronic character of the aryl ligand (**Table 1** and **SI, Table S13;** see **SI, Figure S3** for structural parameter definitions). However, we note that **Os2** has the largest difference between minimum and maximum aryl plane angles for all compounds surveyed here (36.77°, **Table 1**), as well as an unusually low average aryl plane angle (67.45°, where this is 70.12-70.52° for all other compounds; **SI, Table S13**).

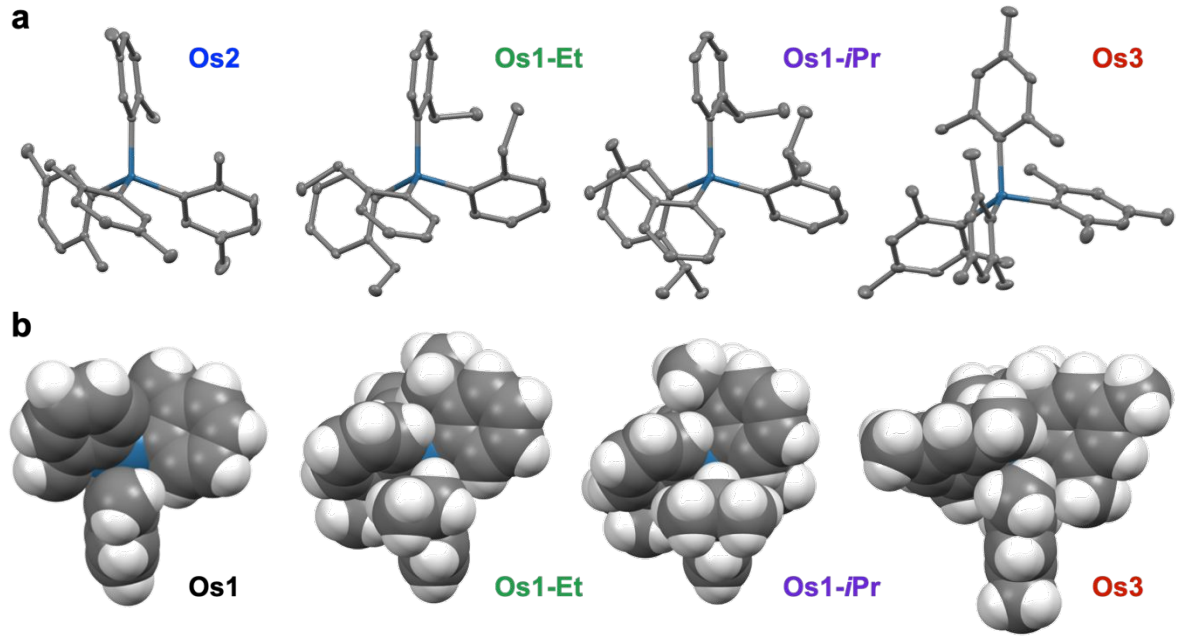

Figure 2. (a) X-ray crystal structures of **Os2**, **Os1-Et**, **Os1-*i*Pr**, and **Os3** (50% probability ellipsoids). Hydrogen atoms are omitted for clarity (Os = teal, C = grey). Selected structural parameters for these and analogous previously characterized tetrahedral compounds are provided in **Table 1** and in the **SI, Tables S13-28**. **(b)** Space filling models of **Os1**,[15] **Os1-Et**, **Os1-*i*Pr**, and **Os3**, illustrating the filling of the pockets that lie directly opposite M-aryl coordination sites (H = white). For **Os1**, **Os1-Et**, and **Os1-*i*Pr**, each of the four pockets is filled with a single methyl, ethyl, or isopropyl group, respectively. For **Os3** each pocket is occupied by two methyl groups, each from a different ligand, providing maximal steric shielding of the Os centre.

Table 1. Selected average and calculated structural parameters for different compounds.

compound	M-C (Å) [a]	aryl plane range (°) [b]	*T*-value [c]	identifier [d]	reference
Os(mesityl)$_4$ (**Os3**)	2.037(3)	18.96	8.02	2024176	this work
Os(cyclohexyl)$_4$	2.029	-	5.18	1135690	[16]
Os(2-^{i}Pr-phenyl) (**Os1-*i*Pr**)	2.015(4)	32.27	5.55	2175534	this work
Os(2-ethylphenyl) (**Os1-Et**)	2.0054(18)	4.28	3.53	2175533	this work
Os(2-tolyl)$_4$ (**Os1**)	1.997	7.51	4.38	1135692	[16]
Os(4-Br-2,5-xylyl)$_4$	2.000(2)	24.87	1.60	164949	[19]
Os(phenyl)$_4$	1.995	24.40	1.32	1153940	[16]
Os(2,5-xylyl)$_4$ (**Os2**)	2.008(4)	36.77	1.11	2024175	this work
Ru(mesityl)$_4$ (**Ru3**)	2.01(1)	17.22	7.42	1191069	[18]
Ru(cyclohexyl)$_4$	2.019	-	4.02	1153943	[16]
Ru(2-tolyl)$_4$ (**Ru1**)	1.995	12.53	3.53	1161553	[17]
Ru(4-MeO-2-tolyl)$_4$	1.986	26.19	2.45	1032104	[38]
Ru(4-Br-2,5-xylyl)$_4$	1.984	24.97	2.17	1032108	[38]
Ru(2,4,5-trimethylphenyl)$_4$	1.985(10)	20.99	0.86	1510576	[39]
C(phenyl)$_4$	1.551	5.98	1.95	191149	[44]

[a] Average bond length, provided with pooled estimated standard deviations (e.s.d.) in parentheses for all structures with associated e.s.d. M = Os, Ru, C. [b] Difference between minimum and maximum aryl plane angles. [c] *T*-value (tetrahedricity) = a measure of the mean absolute deviation of a set of C–M–C angles from their ideal tetrahedral values (109.5°). *T*-value = 0 indicates no deviation. Calculated using **Equation S1**. [d] CCDC Deposition Number.

To simplify comparisons of C-M-C angles we employ a straightforward "tetrahedricity"-value (*T*-value), the root-mean-square deviation of a set of C–M–C angles from their ideal tetrahedral values (109.5°). This is calculated for M(aryl)$_4$ (M = Os, Ru) and related compounds using **Equation S1**, where a *T*-value = 0 indicates no deviation. An analogous "octahedricity" metric has been utilized in the structural characterization of metal polypyridyl complexes;[45–47] and related, yet somewhat more involved analyses have previously been performed for molecular complexes,[48,49] as well as for coordination environments in solid-state materials.[50,51] We observe that *T*-values decrease in the order **M3** > M(cyclohexyl)$_4$ > **M1** for both series of Os and Ru compounds (**Table 1**), suggesting that a greater tetrahedral distortion is required to accommodate aryl ligands of increased steric bulk. The four mesityl groups of **Os3** are arranged in a particularly distorted tetrahedral geometry (*T*-value = 8.02, C-Os-C angles between 98.4-117.2°). This analysis further supports the view that steric constraints due to 2,6-dimethyl substituents contribute to the lower synthetic yield of **Os3** compared to **Os1-2** (**SI, Table S2**). In contrast, complexes with 2,5-xylyl ligands adopt a more

ideal tetrahedral structure compared to **M1** and materials with simple phenyl substituents (**Table 1**). For example, **Os2** (*T*-value = 1.11, C-Os-C angles between 108.6-110.9°) has a more ideal tetrahedral geometry than **Os1** (*T*-value = 4.38), Os(phenyl)$_4$ (*T*-value = 1.32), or C(phenyl)$_4$ (*T*-value = 1.95). While **Os1-Et** has a *T*-value intermediate between **Os1** and **Os2**, **Os1-*i*Pr** has a comparable geometric distortion to Os(cyclohexyl)$_4$.

In **Figure 2b**, we present space-filling models for selected Os(aryl)$_4$ complexes. The specific orientation of these models helps identify a coordination space, or "pocket", which lies directly opposite each M-aryl coordination site. For **Os1**, **Os1-Et**, and **Os1-*i*Pr**, each of the four pockets is filled with a single methyl, ethyl, or isopropyl group, respectively. For **Os3**, each pocket is occupied by two methyl groups, each from a different ligand, providing maximal steric shielding of the Os centre. These models offer a simple rationale for the observed yield trends in terms of the difficulty of arranging each ligand around the Os centre such that all ligand 2- or 2,6-substituents are accommodated in a pocket. It is reasonable to consider whether the well-filled pocket of **Os3** may impart an increased chemical or electrochemical stability to this complex. Unfortunately, preliminary reactivity studies following Arnold *et al.*[52] reveal that black hexane solutions of **Os3** rapidly change colour to yellow upon addition of an excess of PMe_3 (consistent with the formation of the corresponding osmium(II) η^6-biaryl complex), demonstrating that the additional steric shielding imparted by the mesityl ligands does not provide substantial protection against attack by small nucleophiles.

These observations prompted us to explore how commonly used ligand parameters might be utilized to further quantify the steric properties of the σ-aryl ligands studied here. Perhaps the most notable of these parameters is the Tolman cone angle (Θ, readily applied for phosphines), but more recently alternative descriptors such as percentage buried volume (%V_{bur}) have also proven invaluable.[53–56] %V_{bur}, the volume occupied by a ligand within a sphere of typical radius = 3.5 Å from the central metal atom, has, for example, been found to correlate with Θ, facilitating the evaluation of both phosphine and N-heterocyclic carbene ligand steric effects on a common scale.[57] In **Figure 3a**, we illustrate our definition of these metrics for Os(aryl)$_4$ using the 2-ethylphenyl ligand. With Os at the cone apex, and the aryl ring in the x-y plane, we determine Θ_{in} as the sum of the substituent cone angles ($\Theta_{in} = \theta_{in,1} + \theta_{in,2}$, the *in-plane* cone angle), defining $\theta_{in,i}$ between vectors running along the Os-aryl bond (setting this to the average **Os1** bond length, 1.997 Å) and the outermost H-atom centre (not the van der Waals radii). This cone angle definition is similar to one used previously for assessing the steric properties of different cyclopentadienyl ligands, and represents a lower limit.[58] We also determine an *out-of-plane* angle ($\Theta_{out} = \theta_{out,1} + \theta_{out,2}$), as illustrated in **Figure**

3b. This captures additional ligand bulk particularly from *iso*-propyl, and *tert*-butyl substituents. Using these Os-aryl fragment geometries, and the complete Os(aryl)$_4$ geometry obtained from the X-ray crystal structure (where available), we also calculate the %V_{bur} using the SambVca 2.1 web applet (**Figure 3c**; see Experimental Section for details).[37] Parameters for each σ-aryl ligand are provided in **Table 2**. Analysis of these shows that the exclusive use of any single metric cannot fully explain the experimentally observed yield trends. For example, Θ_{in} are similar for tolyl, 2,5-xylyl, and 2-ethylphenyl (for some geometries), as well as for mesityl and 2-*tert*-butylphenyl. However, inclusion of Θ_{out} as a secondary parameter helps delineate the additional bulk of 2-*tert*-butyl groups. While %V_{bur} again cannot be used alone, for example, not easily discriminating between 2-ethyl and 2-*iso*-propyl species, it does further illustrate how sterically congested **Os3** is with %V_{bur} > 85.4. This metric also shows that the 2-*tert*-butylphenyl ligand, with a %V_{bur} = 26.2% for Os-aryl and an estimated %V_{bur} = 104.8% for **Os1-*t*Bu**, is approaching if not exceeding the available ligand volume around the Os centre in Os(aryl)$_4$. Together, these calculated Θ and %V_{bur} values further illustrate why **Os3** is obtained in relative low yields compared to other Os(aryl)$_4$ complexes, and why **Os1-*t*Bu** is synthetically inaccessible. It should be recognized, however, that while the above structural analyses provide a range of useful insights, by focussing exclusively on the final product(s) we overlook the influence of ligand steric properties in key reaction intermediates that may also have significant implications on reaction outcomes.

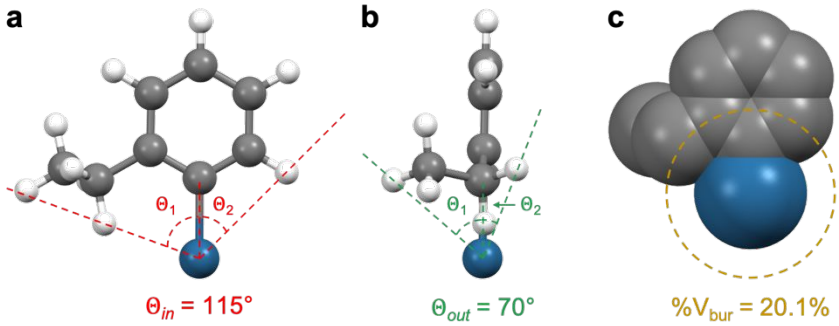

Figure 3. Definition of parameters for σ-aryl ligands in Os(aryl)$_4$ complexes illustrated here for 2-ethyl (this ligand geometry incorporates the average ethyl-aryl dihedral angle from the X-ray crystal structure). Ball and stick models describing **(a)** the *in-plane* ($\Theta_{in} = \theta_{in,1} + \theta_{in,2}$) and **(b)** *out-of-plane* ($\Theta_{out} = \theta_{out,1} + \theta_{out,2}$) cone angles (Os = teal, C = grey, H = white). **(c)** Space-filling model without hydrogens illustrating the calculation of percentage buried volume, %V_{bur}, using the SambVca 2.1 web applet.[37] The dotted circle represents a sphere of radius 3.5 Å. Parameters for each σ-aryl ligand are given in **Table 2**. Schematics showing other Os-aryl geometries are provided in the **SI, Figure S4**.

Table 2. Selected parameters for σ-aryl ligands in Os(aryl)$_4$ complexes.[a]

σ-aryl ligand	Θ_{in} (°)	Θ_{out} (°)	%V_{bur}		
			Os-aryl[b]	Os(aryl)$_4$ calc.[c]	Os(aryl)$_4$ expt.[d]
2-tolyl	109	70	19.8[e]	79.2	76.7
2,5-xylyl	110	70	19.9	79.6	76.7
2-ethylphenyl	109 (115[f])	69 (70[f])	19.8 (20.1[f])	79.2 (80.4[f])	78.8
2-*iso*-propylphenyl	114	98	20.5	82.0	78.7
mesityl	128	70	22.9[g]	91.6	85.4[h]
2-*tert*-butylphenyl	127	149	26.2	104.8	-

[a] *In-plane* angles (Θ_{in}) are calculated using aryl ligand geometries with DFT optimized C-C and C-H bond lengths where 2-substituents have been rotated to minimize Θ_{in}, unless otherwise stated. Os-aryl bond lengths were set to 1.997 Å in each case, the average Os-aryl bond length from the X-ray crystal structure of **Os1**. The *out-of-plane* angles (Θ_{out}) are calculated using the same geometries as for Θ_{in}. [b] Calculated using the *SambVca 2.1* web applet for an Os-aryl fragment having the same geometry as used for Θ_{in} and Θ_{out}, using unscaled (Bondi) van der Waals radii, and with hydrogens excluded from the calculation.[37] [c] Effective calculated %V_{bur} for the Os(aryl)$_4$ complex obtained by multiplying the Os-aryl fragment %V_{bur} by 4. [d] Calculated using the *SambVca 2.1* web applet for the complete Os(aryl)$_4$ complex with atomic coordinates from the X-ray crystal structure, using unscaled (Bondi) van der Waals radii, and with hydrogens excluded from the calculation.[37] [e] Using atomic coordinates for the Os-aryl fragment from the X-ray crystal structure %V_{bur} = 19.2, in good agreement with the calculated values. [f] Θ_{in}, Θ_{out}, and %V_{bur} obtained using a geometry that incorporates the average ethyl-aryl dihedral angle from the X-ray crystal structure. [g] %V_{bur} = 22.5 using an Os-aryl bond length of 2.037 Å, the average Os-aryl bond length from the X-ray crystal structure of **Os3**. [h] %V_{bur} = 88.8% when hydrogens are included in the calculation.

The crystal structures of **Os1-Et** and **Os1-*i*Pr** also proved essential in rationalizing some distinctive features of their ^{1}H NMR spectra. Resonances assigned to the ethyl -C*H*$_3$ groups of **Os1-Et**, and one of the two *iso*-propyl -C*H*$_3$ groups of **Os1-*i*Pr** (usually appearing as a single -CH$_3$ resonance), are observed at unusually low chemical shifts (**Figure 4a** and **b**; δ = 0.52 and 0.23 ppm, respectively). As shown in **Figure 4c**, the coordination geometry of these Os(aryl)$_4$ complexes helps to centrally position the protons of these groups over the face centre of an adjacent σ-aryl ligand. We propose these proton environments experience additional inter-ligand *shielding* effects due to aromatic ring currents, significantly shifting their resonances upfield relative to those of the bromoaryl ligand precursors (**Figure 4a** and **b**; δ = 1.26 and 1.22 ppm, respectively). While rotation about the Os-aryl, aryl-Et/*i*Pr, and C-CH$_3$ bonds will serve to modulate inter-ligand bond distances and interactions in solution, in the solid state we find that the average distances between aryl centroids and their closest -CH$_3$

protons are 2.84 and 2.91 Å for **Os1-Et** and **Os1-*i*Pr**, respectively. Our findings are consistent with the expected inverse relationship between aryl centroid-proton distance and upfield chemical shift, and in line with experimental findings for prototypical compounds demonstrating such effects.[59] Indeed, aryl centroid-proton distances (upfield chemical shifts) for these $Os(aryl)_4$ complexes are large (small) compared to the 1.64 Å distance ($\delta_H = -4.08$ ppm) found in an adamantyl-bridged [7]paracyclophane,[60] or the 2.13 Å distance ($\delta_H = -2.74$ ppm) for a trisulfone-bridged C_3 symmetric cyclophane.[61]

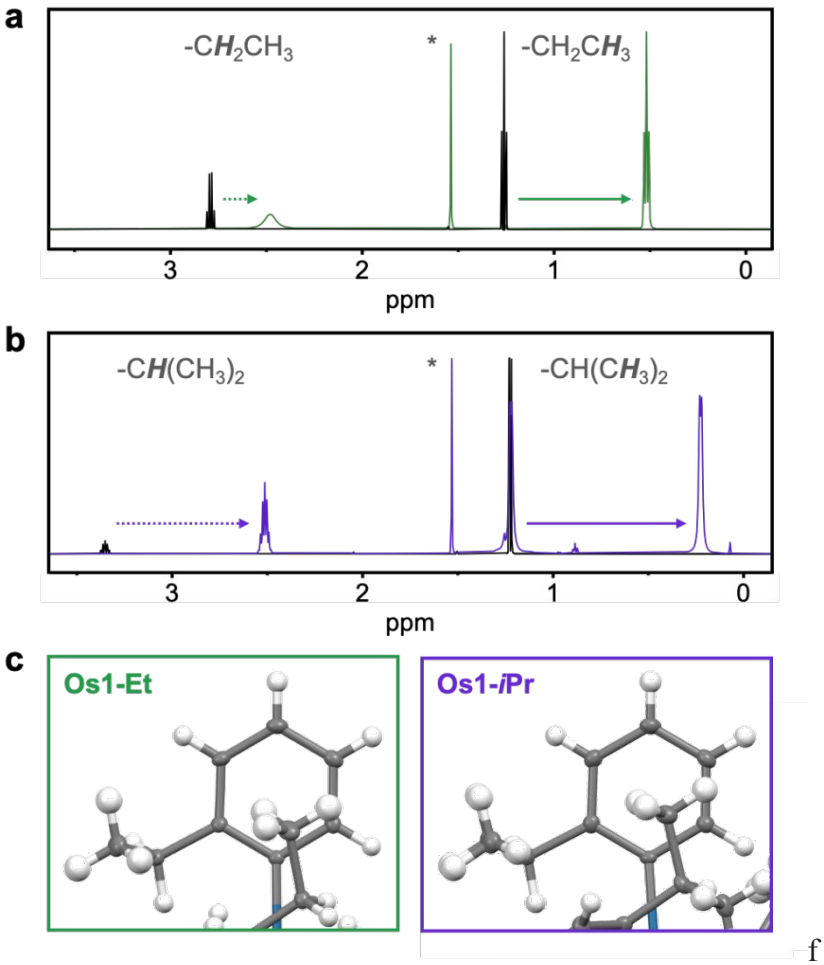

Figure 4. Overlaid ^{1}H NMR spectra in $CDCl_3$ (600 MHz) showing the chemical shift changes for aryl 2-substituent proton resonances between the bromoaryl ligand precursors and Os(aryl)$_4$ for **(a)** 2-ethylphenyl and **(b)** 2-*iso*-propylphenyl compounds. Solid arrows indicate the -C*H*$_3$ resonance shifts we attribute predominantly to intra-ligand aromatic ring current effects (note that only one ^{i}Pr -CH$_3$ group experiences an upfield shift in **Os1-*i*Pr**). While the chemical shifts of these resonances are also influenced by inductive effects upon changing Br-aryl to Os-aryl, the observed changes for -C*H*$_3$ proton resonances are larger than those observed for the corresponding, more proximal, -C*H*$_2$CH$_3$ or -C*H*(CH$_3$) resonances (dotted arrows). This indicates the significant -C*H*$_3$ resonance upfield shifts cannot be solely attributed to inductive effects. **(c)** Ball and stick models of the **Os1-Et** and **Os1-*i*Pr** crystal structures (partial view, perpendicular to an aryl plane) showing the orientation of ligand -CH$_3$ groups close to the aryl centroid in these complexes.

The significant influence of aryl substituents on Os(aryl)$_4$ yields motivated further studies of **Os1-3**, **Os1-Et** and **Os1-*i*Pr** by cyclic voltammetry to probe substituent effects on their electrochemical properties. The results are summarized in **Table 3** and **SI, Table S29**, with representative overlaid cyclic voltammograms shown in **Figure 5**. Voltammograms for **Os3** at different scan rates are shown in **SI, Figure S5**. All complexes exhibit two reversible, one-electron transfers ($i_{pa}/i_{pc} \approx 1$, $i_p \propto V_s^{1/2}$), in broad agreement with previous reports.[21,22] These 0/1+ and 1−/0 events have previously been assigned to the Os^{4+}/Os^{5+} and Os^{3+}/Os^{4+} redox couples, respectively. Interestingly, we observe an additional 1+/2+ oxidation event for **Os3** at +1.117 V which may be metal Os^{5+}/Os^{6+} or ligand-based.[21] Using the equilibrium potentials for the 0/1+ feature of **Os1-3**, we find that these Os(aryl)$_4$ complexes are approximately ~22 mV easier to oxidize for every methyl substituent added. In addition, the 1−/0 feature shifts to more negative potentials by ~20-50 mV/methyl. This is compared to ~50 mV/methyl group for ferrocene analogues.[62] Extrapolating from these values, we estimate the 0/1+ equilibrium potential of Os(2,3,4,5,6-pentamethylphenyl)$_4$ (**Os5**) to be around −0.02 mV vs. $[Cp_2Fe]^+/[Cp_2Fe]$, with a total range of ~350 mV between the mono-substituted and permethylated complexes (4-20 methyl substituents). This range is somewhat smaller than the ~500 mV potential difference between ferrocene and decamethylferrocene (0-10 methyl substituents). In contrast, variation of the alkyl substituent at the 2-position in **Os1**, **Os1-Et**, and **Os1-*i*Pr** has no clear influence on the 0/1+ equilibrium potential (changing over a total range of only ~20 mV), but systematically shifts the 1−/0 feature to more negative potentials by ~50-70 mV with each substitution of a C-*H* group for C-*CH$_3$*. Taken together, this data shows that judicious selection of aryl ligand substituents is capable of independently tuning the LUMO energy level of Os(aryl)$_4$, or modulating both HOMO and LUMO energy levels simultaneously.

Table 3. Selected electrochemical data for $Os(aryl)_4$ complexes.[a]

entry	compound	solvent	$E_{1/2}$ (V)				reference
			2−/1−	1−/0	0/1+	1+/2+	
1 [b]	$Os(2\text{-tolyl})_4$ (**Os1**)	THF	−2.47	−1.89	+0.41	-	[21]
2 [b]		CH_2Cl_2	-	−1.96	+0.33	-	[21]
3		CH_2Cl_2	-	−1.961	+0.326	-	this work
4 [c]	$Os(2,5\text{-xylyl})_4$ (**Os2**)	CH_2Cl_2	-	−1.48 [d]	+0.24	-	[22]
5		CH_2Cl_2	-	−2.008	+0.244	-	this work
6	$Os(mesityl)_4$ (**Os3**)	CH_2Cl_2	-	−2.028	+0.153	+1.117	this work
7	$Os(2\text{-ethylphenyl})_4$ (**Os1-Et**)	CH_2Cl_2	-	−2.026	+0.349	-	this work
8	$Os(2\text{-}i\text{Pr-phenyl})_4$ (**Os1-*i*Pr**)	CH_2Cl_2	-	−2.075	+0.336	-	this work

[a] Scan rate = 0.1 V s^{-1}; NBu_4PF_6 supporting electrolyte; working electrode: glassy carbon; reference electrode, counter electrode: Pt. Potentials measured with internal Cp^*_2Fe (−0.532 V vs $[Cp_2Fe]^+/[Cp_2Fe]$),[62] reported relative to $[Cp_2Fe]^+/[Cp_2Fe]$. See **SI, Table S29** for additional electrochemical data. [b] Scan rate = 0.05 V s^{-1}; working electrode: Pt; reference electrode: Ag; counter electrode: W. Potentials measured with internal Cp_2Fe. [c] Reference electrode: $Ag/AgNO_3$ (0.1 M in acetonitrile). Potentials measured with internal Cp_2Fe. [d] The reported potential of the 1−/0 redox event is significantly shifted compared to other measurements for these compounds.

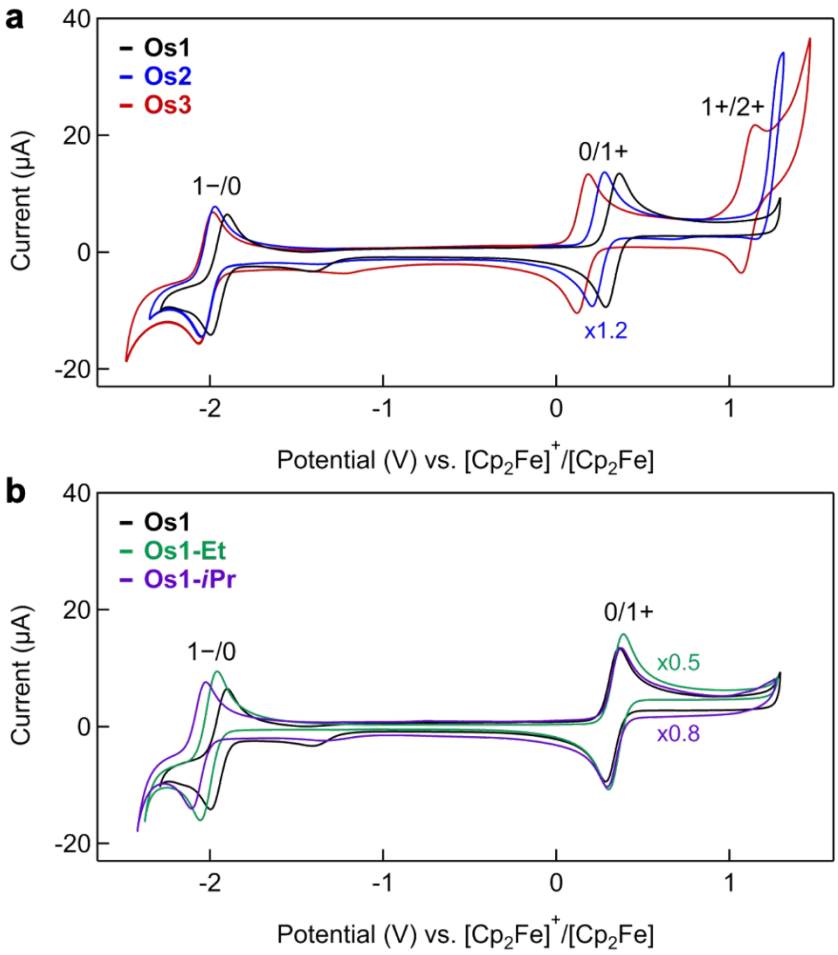

Figure 5. Solution cyclic voltammograms of Os(aryl)$_4$ in 0.1 M NBu_4PF_6–CH_2Cl_2. Potentials are reported relative to FcH/[FcH]$^+$, corrected for iR_u. Scan rate = 0.1 V s^{-1}. **(a)** Overlaid voltammograms for Os(2-tolyl)$_4$ (**Os1**, black), Os(2,5-xylyl)$_4$ (**Os2**, blue), and Os(mesityl)$_4$ (**Os3**, red) show redox features are shifted to more negative potentials with increasing numbers of methyl substituents. A second oxidation event (1+/2+) is observed for **Os3**. **(b)** Overlaid voltammograms for **Os1** (black), Os(2-ethylphenyl)$_4$ (**Os1-Et**, green), Os(2-*iso*-propylphenyl)$_4$ (**Os1-*i*Pr**, purple) show that increasing the bulk/electron-donating character of the 2-substituent has a minimal influence on the 0/1+ redox potential but successively shifts the 1−/0 feature to more negative potentials.

CONCLUSIONS

We have shown that synthetic yields of Os(aryl)$_4$ complexes can be significantly improved using the new starting material $(Oct_4N)_2[OsBr_6]$, even facilitating the preparation of previously inaccessible compounds such as **Os3**. $(Oct_4N)_2[OsBr_6]$ is non-hazardous,

straightforward to prepare, and convenient to handle, avoiding the direct use of volatile and toxic OsO_4 in reactions with aryl Grignard reagents. Despite these advantages ligand choice remains critical, where the incorporation of 2,6-disubstituted ligands, or those with sterically bulky 2-substituents, significantly diminishes yields of the corresponding $Os(aryl)_4$ compound. This is rationalized through analysis of various ligand parameters, as well as single-crystal X-ray diffraction structures for differently substituted $Os(aryl)_4$ which reveal that 2- or 2,6-substituents must fit inside a pocket of limited volume within the metal coordination sphere. As illustrated by **Os3**, occupation of the available pocket volume may require distortion of the tetrahedral coordination geometry, the extent of which can be quantified using a straightforward "tetrahedricity" metric. The synthesis of **Os1-*t*Bu**, having an estimated $\%V_{bur} \gtrsim 100\%$, is severely sterically inhibited.

Solution voltammograms of **Os1-3, Os1-Et**, and **Os1-*i*Pr** illustrate how the redox properties of $Os(aryl)_4$, with 20 possible substituent positions, can be readily tuned. Differences in ligand steric bulk, or complex tetrahedricity, do not appear to negatively impact the reversibility of these electrochemical processes. We recognize that the robust redox properties of $Os(aryl)_4$,[21] the stability of $M(aryl)_4$ complexes with different metal centres,[1] and the potential for direct functionalization of their σ-aryl ligands[19,20] draw intriguing parallels with metallocenes, the well-established and broadly utilized prototypical family of organometallic complexes. It is hoped that this work will help inspire further studies of this fascinating class of tetrahedral materials towards applications where such organometallic complexes have already demonstrated utility, for example in sensing, catalysis, or as components of extended molecular systems such as polymers or supramolecular assemblies.[63,64]

ASSOCIATED CONTENT

Electronic Supplementary Information (ESI) available: Additional synthetic information, infrared spectra, ^{1}H and $^{13}C\{^{1}H\}$ NMR spectra for all new compounds, X-ray crystal structure data for **Os2**, **Os3**, **Os1-Et**, **Os1-*i*Pr**, and $OsO_2(mes)_2$ (CCDC 2024175, 2024176, 2175533, 2175534, 2119165), details of tetrahedricity calculations and additional structural information for the compounds detailed in **Table 1**, σ-aryl ligand geometries, and solution electrochemical data for **Os1-3**, **Os1-Et**, **Os1-*i*Pr**.

AUTHOR INFORMATION

Corresponding Author

Michael S. Inkpen – Email: inkpen@usc.edu

Conflicts of Interest

There are no conflicts of interest to declare.

ACKNOWLEDGEMENTS

This work was primarily supported by University of Southern California (USC) startup funds. J.M.P. and C.O. are grateful for additional support from USC Wrigley Institute for Environmental Studies Norma and Jerol Sonosky Environmental Sustainability Graduate Summer Fellowships. We thank Narcisse Ukwitegetse, Tian-Yi Li, and Mattia Di Niro for help with CHN experiments, and Nils Rotthowe for useful comments and mass spectrometry analyses. We thank the NSF (DBI-0821671, CHE-0840366, CHE-1048807, CHE-2018740) and the NIH (S10 RR25432) for analytical instrumentation. The authors thank John Arnold (University of California, Berkeley) for valuable discussions.

REFERENCES

(1) Koschmieder, S. U.; Wilkinson, G. Homoleptic and Related Aryls of Transition Metals. *Polyhedron* **1991**, *10* (2), 135–173.

(2) El-Kaderi, H. M.; Hunt, J. R.; Mendoza-Cortés, J. L.; Côté, A. P.; Taylor, R. E.; O'Keeffe, M.; Yaghi, O. M. Designed Synthesis of 3D Covalent Organic Frameworks. *Science* **2007**, *316* (5822), 268–272.

(3) Dincă, M.; Dailly, A.; Long, J. R. Structure and Charge Control in Metal-Organic Frameworks Based on the Tetrahedral Ligand Tetrakis(4-Tetrazolylphenyl)Methane. *Chem. Eur. J.* **2008**, *14* (33), 10280–10285.

(4) Muller, T.; Bräse, S. Tetrahedral Organic Molecules as Components in Supramolecular Architectures and in Covalent Assemblies, Networks and Polymers. *RSC Adv.* **2014**, *4* (14), 6886–6907.

(5) Yaghi, O. M.; Kalmutzki, M. J.; Diercks, C. S. *Introduction to Reticular Chemistry: Metal-Organic Frameworks and Covalent Organic Frameworks*, 1st ed.; Wiley Online Books; Wiley-VCH Verlag GmbH & Co. KGaA: Weinheim, Germany, 2019.

(6) Monnereau, L.; Nieger, M.; Muller, T.; Bräse, S. Tetrakis-(4-Thiyphenyl)Methane: Origin of a Reversible 3D-Homopolymer. *Adv. Funct. Mater.* **2014**, *24* (8), 1054–1058.

(7) Hirayama, D.; Takimiya, K.; Aso, Y.; Otsubo, T.; Hasobe, T.; Yamada, H.; Imahori, H.; Fukuzumi, S.; Sakata, Y. Large Photocurrent Generation of Gold Electrodes Modified with [60]Fullerene-Linked Oligothiophenes Bearing a Tripodal Rigid

Anchor. *J. Am. Chem. Soc.* **2002**, *124* (4), 532–533.

(8) Valášek, M.; Edelmann, K.; Gerhard, L.; Fuhr, O.; Lukas, M.; Mayor, M. Synthesis of Molecular Tripods Based on a Rigid 9,9′-Spirobifluorene Scaffold. *J. Org. Chem.* **2014**, *79* (16), 7342–7357.

(9) Lindner, M.; Valášek, M.; Homberg, J.; Edelmann, K.; Gerhard, L.; Wulfhekel, W.; Fuhr, O.; Wächter, T.; Zharnikov, M.; Kolivoška, V.; Pospíšil, L.; Mészáros, G.; Hromadová, M.; Mayor, M. Importance of the Anchor Group Position (Para versus Meta) in Tetraphenylmethane Tripods: Synthesis and Self-Assembly Features. *Chem. Eur. J.* **2016**, *22*, 13218–13235.

(10) Valášek, M.; Lindner, M.; Mayor, M. Rigid Multipodal Platforms for Metal Surfaces. *Beilstein J. Nanotechnol.* **2016**, *7* (1), 374–405.

(11) Karimi, M. A.; Bahoosh, S. G.; Valášek, M.; Bürkle, M.; Mayor, M.; Pauly, F.; Scheer, E.; Agraït, N.; Cuevas, J. C.; Mikkelsen, K. V. Identification of the Current Path for a Conductive Molecular Wire on a Tripodal Platform. *Nanoscale* **2016**, *8* (20), 10582–10590.

(12) Gerhard, L.; Edelmann, K.; Homberg, J.; Valášek, M.; Bahoosh, S. G.; Lukas, M.; Pauly, F.; Mayor, M.; Wulfhekel, W. An Electrically Actuated Molecular Toggle Switch. *Nature Commun.* **2017**, *8*, 14672.

(13) Bayliss, S. L.; Laorenza, D. W.; Mintun, P. J.; Kovos, B. D.; Freedman, D. E.; Awschalom, D. D. Optically Addressable Molecular Spins for Quantum Information Processing. *Science* **2020**, *370* (6522), 1309–1312.

(14) Laorenza, D. W.; Kairalapova, A.; Bayliss, S. L.; Goldzak, T.; Greene, S. M.; Weiss, L. R.; Deb, P.; Mintun, P. J.; Collins, K. A.; Awschalom, D. D.; Berkelbach, T. C.; Freedman, D. E. Tunable Cr^{4+} Molecular Color Centers. *J. Am. Chem. Soc.* **2021**, *143* (50), 21350–21363.

(15) Tooze, R. P.; Stavropoulos, P.; Motevalli, M.; Hursthouse, M. B.; Wilkinson, G. Synthesis and X-Ray Crystal Structures of the First Tetrahedral Osmium(IV) Compounds, Tetrakis(Cyclohexyl)Osmium(IV) and Tetrakis(*o*-Methylphenyl)Osmium(IV). *J. Chem. Soc. Chem. Commun.* **1985**, 1139–1140.

(16) Stavropoulos, P.; Savage, P. D.; Tooze, R. P.; Wilkinson, G.; Hussain, B.; Motevalli, M.; Hursthouse, M. B. The Synthesis and X-Ray Crystal Structures of Homoleptic Tetrahedral Aryls of Osmium(IV) and of Cyclohexyls of Ruthenium(IV), Osmium(IV), and Chromium(IV). *Dalton Trans.* **1987**, *3*, 557–562.

(17) Savage, P. D.; Wilkinson, G.; Motevalli, M.; Hursthouse, M. B. Synthesis of

Homoleptic Tetrahedral Aryls of Rhenium(IV) and Ruthenium(IV). X-Ray Crystal Structures of Tetrakis(o-Methylphenyl)Rhenium(IV), Tetrakis(*o*-Methylphenyl)Oxorhenium(VI), and Tetrakis(*o*-Methylphenyl)-Ruthenium(IV). *Dalton Trans.* **1988**, *3*, 669–673.

(18) Hay-Motherwell, R.; Wilkinson, G.; Hussain-Bates, B.; Hurthouse, M. Homoleptic Mesityls of Iridium(III,IV,V) and Ruthenium(IV,V). *Dalton Trans.* **1992**, 3477–3482.

(19) Lau, M. K.; Zhang, Q. F.; Chim, J. L. C.; Wong, W. T.; Leung, W. H. Direct Functionalisation of σ-Aryl Ligands: Preparation of Homoleptic Functionalised Aryls of Osmium(IV). *Chem. Commun.* **2001**, *1* (16), 1478–1479.

(20) Savage, P. D. Organometallic Compounds of Rhenium and the Platinum Group Metals, Ph.D. Thesis, Imperial College of Science & Technology, 1987.

(21) Arnold, J.; Wilkinson, G.; Hussain, B.; Hursthouse, M. B. Redox Chemistry of the Homoleptic Aryl $Os(2\text{-}MeC_6H_4)_4$: Synthesis and Characterization of the First Osmium(V) Organometallic $[Os(2\text{-}MeC_6H_4)_4][CF_3SO_3]$. *J. Chem. Soc. Chem. Commun.* **1988**, *20*, 1349–1350.

(22) Lau, M.-K.; Chim, J. L.; Wong, W.-T.; Williams, I. D.; Leung, W.-H. Synthesis and Molecular Structures of Monooxo Aryl Complexes of Osmium(VI). *Can. J. Chem.* **2001**, *79* (5–6), 607–612.

(23) Stravropoulos, P.; Edwards, P. G.; Behling, T.; Wilkinson, G.; Motevalli, M.; Hursthouse, M. B. Oxoaryls of Rhenium-(V) and -(VI) and Osmium(VI). X-Ray Crystal Structures of Dimesityldioxorhenium(VI), Tetramesityloxorhenium(VI), and Dimesityldioxoosmium(VI). *Dalton Trans.* **1987**, *1*, 169–175.

(24) Dwyer, F. P.; Hogarth, J. W.; Rhoda, R. N. Ammonium Hexabromoosmate (IV). *Inorg. Synth.* **1957**, *5*, 204–206.

(25) Love, B. E.; Jones, E. G. The Use of Salicylaldehyde Phenylhydrazone as an Indicator for the Titration of Organometallic Reagents. *J. Org. Chem.* **1999**, *64* (10), 3755–3756.

(26) Rodriguez, J. R.; Félix, R. M.; Reynoso, E. A.; Fuentes Moyado, S.; Alonso-Núñez, G. Coordination Complex Synthesis of Noble Metals in the Preparation of Nanoparticles Supported on MWCNTs Used as Electrocatalysts. *Inorganica Chim. Acta* **2013**, *406*, 138–145.

(27) Dwyer, F. P.; Hogarth, J. W.; Rhoda, R. N. Ammonium Hexachloroosmate (IV). In *Inorg. Synth.*; Moeller, T., Ed.; 1957; Vol. 5, pp 206–207.

(28) Dwyer, F. P.; Hogarth, J. W.; Rhoda, R. N. Ammonium Hexabromoosmate (IV). In *Inorg. Synth.*; Moeller, T., Ed.; 1957; Vol. 5, pp 204–206.

(29) Fulmer, G. R.; Miller, A. J. M.; Sherden, N. H.; Gottlieb, H. E.; Nudelman, A.; Stoltz, B. M.; Bercaw, J. E.; Goldberg, K. I. NMR Chemical Shifts of Trace Impurities: Common Laboratory Solvents, Organics, and Gases in Deuterated Solvents Relevant to the Organometallic Chemist. *Organometallics* **2010**, *29* (9), 2176–2179.

(30) Berger, S.; Braun, S. *200 and More NMR Experiments*, 2nd Ed.; Wiley-VCH Verlag GmbH & Co. KGaA: Weinheim, Germany, 2004.

(31) Hardy, D. T.; Wilkinson, G.; Young, G. B. Mechanistic Studies of Ligand-Induced Thermolytic Reductive Elimination of Biaryl from Tetraarylosmium(IV). *Polyhedron* **1996**, *15* (8), 1363–1373.

(32) SHELXTL 2014/7, Bruker AXS, Madison, WI, 2014.

(33) Sheldrick, G. M. SHELX-97. *Acta Crystallogr., Sect. A* **2008**, *64*, 112–122.

(34) Sheldrick, G. M. Crystal Structure Refinement with SHELXL. *Acta Crystallogr., Sect. C* **2015**, *71* (1), 3–8.

(35) Hübschle, C. B.; Sheldrick, G. M.; Dittrich, B. ShelXle: A Qt Graphical User Interface for SHELXL. *J. Appl. Crystallogr.* **2011**, *44*, 1281–1284.

(36) Epifanovsky, E.; Gilbert, A. T. B.; Feng, X.; Lee, J.; Mao, Y.; Mardirossian, N.; Pokhilko, P.; White, A. F.; Coons, M. P.; Dempwolff, A. L.; Gan, Z.; Hait, D.; Horn, P. R.; Jacobson, L. D.; Kaliman, I.; Kussmann, J.; Lange, A. W.; Lao, K. U.; Levine, D. S.; Liu, J.; McKenzie, S. C.; Morrison, A. F.; Nanda, K. D.; Plasser, F.; Rehn, D. R.; Vidal, M. L.; You, Z. Q.; Zhu, Y.; Alam, B.; Albrecht, B. J.; Aldossary, A.; Alguire, E.; Andersen, J. H.; Athavale, V.; Barton, D.; Begam, K.; Behn, A.; Bellonzi, N.; Bernard, Y. A.; Berquist, E. J.; Burton, H. G. A.; Carreras, A.; Carter-Fenk, K.; Chakraborty, R.; Chien, A. D.; Closser, K. D.; Cofer-Shabica, V.; Dasgupta, S.; De Wergifosse, M.; Deng, J.; Diedenhofen, M.; Do, H.; Ehlert, S.; Fang, P. T.; Fatehi, S.; Feng, Q.; Friedhoff, T.; Gayvert, J.; Ge, Q.; Gidofalvi, G.; Goldey, M.; Gomes, J.; González-Espinoza, C. E.; Gulania, S.; Gunina, A. O.; Hanson-Heine, M. W. D.; Harbach, P. H. P.; Hauser, A.; Herbst, M. F.; Hernández Vera, M.; Hodecker, M.; Holden, Z. C.; Houck, S.; Huang, X.; Hui, K.; Huynh, B. C.; Ivanov, M.; Jász, Á.; Ji, H.; Jiang, H.; Kaduk, B.; Kähler, S.; Khistyaev, K.; Kim, J.; Kis, G.; Klunzinger, P.; Koczor-Benda, Z.; Koh, J. H.; Kosenkov, D.; Koulias, L.; Kowalczyk, T.; Krauter, C. M.; Kue, K.; Kunitsa, A.; Kus, T.; Ladjánszki, I.; Landau, A.; Lawler, K. V.; Lefrancois, D.; Lehtola, S.; Li, R. R.; Li, Y. P.; Liang, J.; Liebenthal, M.; Lin, H. H.; Lin, Y. S.; Liu, F.; Liu, K. Y.; Loipersberger, M.; Luenser, A.; Manjanath, A.; Manohar, P.; Mansoor, E.; Manzer, S. F.; Mao, S. P.; Marenich, A. V.; Markovich, T.;

Mason, S.; Maurer, S. A.; McLaughlin, P. F.; Menger, M. F. S. J.; Mewes, J. M.; Mewes, S. A.; Morgante, P.; Mullinax, J. W.; Oosterbaan, K. J.; Paran, G.; Paul, A. C.; Paul, S. K.; Pavošević, F.; Pei, Z.; Prager, S.; Proynov, E. I.; Rák, Á.; Ramos-Cordoba, E.; Rana, B.; Rask, A. E.; Rettig, A.; Richard, R. M.; Rob, F.; Rossomme, E.; Scheele, T.; Scheurer, M.; Schneider, M.; Sergueev, N.; Sharada, S. M.; Skomorowski, W.; Small, D. W.; Stein, C. J.; Su, Y. C.; Sundstrom, E. J.; Tao, Z.; Thirman, J.; Tornai, G. J.; Tsuchimochi, T.; Tubman, N. M.; Veccham, S. P.; Vydrov, O.; Wenzel, J.; Witte, J.; Yamada, A.; Yao, K.; Yeganeh, S.; Yost, S. R.; Zech, A.; Zhang, I. Y.; Zhang, X.; Zhang, Y.; Zuev, D.; Aspuru-Guzik, A.; Bell, A. T.; Besley, N. A.; Bravaya, K. B.; Brooks, B. R.; Casanova, D.; Chai, J. Da; Coriani, S.; Cramer, C. J.; Cserey, G.; Deprince, A. E.; Distasio, R. A.; Dreuw, A.; Dunietz, B. D.; Furlani, T. R.; Goddard, W. A.; Hammes-Schiffer, S.; Head-Gordon, T.; Hehre, W. J.; Hsu, C. P.; Jagau, T. C.; Jung, Y.; Klamt, A.; Kong, J.; Lambrecht, D. S.; Liang, W.; Mayhall, N. J.; McCurdy, C. W.; Neaton, J. B.; Ochsenfeld, C.; Parkhill, J. A.; Peverati, R.; Rassolov, V. A.; Shao, Y.; Slipchenko, L. V.; Stauch, T.; Steele, R. P.; Subotnik, J. E.; Thom, A. J. W.; Tkatchenko, A.; Truhlar, D. G.; Van Voorhis, T.; Wesolowski, T. A.; Whaley, K. B.; Woodcock, H. L.; Zimmerman, P. M.; Faraji, S.; Gill, P. M. W.; Head-Gordon, M.; Herbert, J. M.; Krylov, A. I. Software for the Frontiers of Quantum Chemistry: An Overview of Developments in the Q-Chem 5 Package. *J. Chem. Phys.* **2021**, *155* (8).

(37) Falivene, L.; Cao, Z.; Petta, A.; Serra, L.; Poater, A.; Oliva, R.; Scarano, V.; Cavallo, L. Towards the Online Computer-Aided Design of Catalytic Pockets. *Nature. Chem.* **2019**, *11* (10), 872–879.

(38) So, S. C.; Cheung, W. M.; Wang, G. C.; Kwan Huang, E.; Lau, M. K.; Zhang, Q. F.; Sung, H. H. Y.; Williams, I. D.; Leung, W. H. Migratory Insertion and Reductive Coupling of Tetraarylruthenium(IV) Complexes. *Organometallics* **2014**, *33* (17), 4497–4502.

(39) Wang, C.-J.; Wu, X.-L.; Ma, X.-F.; Jia, A.-Q.; Zhang, Q.-F. Synthesis and Crystal Structure of a New Homoleptic Tetraarylruthenium(IV) Complex Ru(2,4,5-$Me_3C_6H_2)_4$. *Z. Naturforsch* **2017**, *72* (7), 523–525.

(40) Deeth, R. J.; Jenkins, H. D. B. A Density Functional and Thermochemical Study of M-X Bond Lengths and Energies in $[MX_6]^{2-}$ Complexes: LDA versus Becke88/Perdew86 Gradient-Corrected Functionals. *J. Phys. Chem. A* **1997**, *101* (26), 4793–4798.

(41) Falivene, L.; Poater, A.; Cazin, C. S. J.; Slugovc, C.; Cavallo, L. Energetics of the Ruthenium-Halide Bond in Olefin Metathesis (Pre)Catalysts. *Dalton Trans.* **2013**, *42*

(20), 7312–7317.

(42) Longley, C. J.; Savage, P. D.; Wilkinson, G.; Hussain, B.; Hurthouse, M. Alkylimido and Oxo Aryls of Rhenium. X-Ray Structures of $(ButN)_2ReCl_2(o\text{-}MeC_6H_4)$ and $MO_2(2,6\text{-}Me_2C_6H_3)_2$, M = Re and Os. *Polyhedron* **1988**, *7* (12), 1079–1088.

(43) Hay-Motherwell, R. S.; Wilkinson, G.; Hussain-Bates, B.; Hursthouse, M. B. Homoleptic Mesityls of Iridium(III,IV,V) and Ruthenium(IV,V). *Dalton Trans.* **1992**, 3477-3482.

(44) Knop, O.; Rankin, K. N.; Cameron, T. S.; Boyd, R. J. Crystal Chemistry of Tetraradial Species. Part 10. Tilting at Windmills: Conformations of the Tetraphenyl Species $ZPh_4^{0,\pm1}$ (Z = B, C, N). *Can. J. Chem.* **2002**, *80* (10), 1351–1366.

(45) Brown, C. M.; Arsenault, N. E.; Cross, T. N. K.; Hean, D.; Xu, Z.; Wolf, M. O. Structural, Electrochemical and Photophysical Behavior of Ru(II) Complexes with Large Bite Angle Sulfur-Bridged Terpyridyl Ligands. *Inorg. Chem. Front.* **2020**, *7*, 117–127.

(46) Österman, T.; Abrahamsson, M.; Becker, H.-C.; Hammarström, L.; Persson, P. Influence of Triplet State Multidimensionality on Excited State Lifetimes of Bis-Tridentate RuII Complexes: A Computational Study. *J. Phys. Chem. A* **2012**, *116* (3), 1041–1050.

(47) Lundqvist, M. J. Quantum Chemical Modeling of Dye-Sensitized Titanium Dioxide: Ruthenium Polypyridyl and Perylene Dyes, TiO_2 Nanoparticles, and Their Interfaces, Ph.D. Thesis, Uppsala University, 2006.

(48) Heard, G. L.; Gillespie, R. J.; Rankin, D. W. H. Ligand Close Packing and the Geometries of $A(XY)_4$ and Some Related Molecules. *J. Mol. Struct.* **2000**, *520* (1–3), 237–248.

(49) Cirera, J.; Alemany, P.; Alvarez, S. Mapping the Stereochemistry and Symmetry of Tetracoordinate Transition-Metal Complexes. *Chem. Eur. J.* **2004**, *10* (1), 190–207.

(50) Hiwatari, Y.; Saito, T.; Ueda, A. Structural Characterization of Soft-Core and Hard-Core Glasses by Delaunay Tessellation. *J. Chem. Phys.* **1984**, *81* (12), 6044–6050.

(51) Medvedev, N. N.; Naberukhin, Y. I. Shape of the Delaunay Simplices in Dense Random Packings of Hard and Soft Spheres. *J. Non. Cryst. Solids* **1987**, *94* (3), 402–406.

(52) Arnold, J.; Wilkinson, G.; Hussain, B.; Hursthouse, M. B. Reactivity of the Homoleptic Osmium Aryl $Os(2\text{-}MeC_6H_4)_4$: Ligand-Induced Reductive Coupling, Sigma- to Pi-Rearrangement, and Ortho-Hydrogen Activation. *Organometallics* **1989**,

8 (5), 1362–1369.

(53) Hillier, A. C.; Sommer, W. J.; Yong, B. S.; Petersen, J. L.; Cavallo, L.; Nolan, S. P. A Combined Experimental and Theoretical Study Examining the Binding of N-Heterocyclic Carbenes (NHC) to the Cp*RuCl (Cp* = η^5-C_5Me_5) Moiety: Insight into Stereoelectronic Differences between Unsaturated and Saturated NHC Ligands. *Organometallics* **2003**, *22* (21), 4322–4326.

(54) Poater, A.; Cosenza, B.; Correa, A.; Giudice, S.; Ragone, F.; Scarano, V.; Cavallo, L. SambVca: A Web Application for the Calculation of the Buried Volume of N-Heterocyclic Carbene Ligands. *Eur. J. Inorg. Chem.* **2009**, No. 13 SPEC. ISS., 1759–1766.

(55) Falivene, L.; Credendino, R.; Poater, A.; Petta, A.; Serra, L.; Oliva, R.; Scarano, V.; Cavallo, L. SambVca 2. A Web Tool for Analyzing Catalytic Pockets with Topographic Steric Maps. *Organometallics* **2016**, *35* (13), 2286–2293.

(56) Wu, K.; Doyle, A. G. Parameterization of Phosphine Ligands Demonstrates Enhancement of Nickel Catalysis via Remote Steric Effects. *Nature. Chem.* **2017**, *9* (8), 779–784.

(57) Clavier, H.; Nolan, S. P. Percent Buried Volume for Phosphine and N-Heterocyclic Carbene Ligands: Steric Properties in Organometallic Chemistry. *Chem. Commun.* **2010**, *46* (6), 841–861.

(58) Glöckner, A.; Bauer, H.; Maekawa, M.; Bannenberg, T.; Daniliuc, C. G.; Jones, P. G.; Sun, Y.; Sitzmann, H.; Tamm, M.; Walter, M. D. How Big Is a Cp? Cycloheptatrienyl Zirconium Complexes with Bulky Cyclopentadienyl and Indenyl Ligands. *Dalton Trans.* **2012**, *41* (22), 6614–6624.

(59) Pascal, R. A. Molecular "Iron Maidens": Ultrashort Nonbonded Contacts in Cyclophanes and Other Crowded Molecules. *European J. Org. Chem.* **2004**, No. 18, 3763–3771.

(60) Lemmerz, R.; Nieger, M.; Vögtle, F. New Highly Strained Adamantanophanes. *J. Chem. Soc. Chem. Commun.* **1993**, No. 14, 1168–1170.

(61) Pascal, R. A.; Grossman, R. B.; Van Engen, D. Synthesis of In-[34,10][7]Metacyclophane: Projection of an Aliphatic Hydrogen toward the Center of an Aromatic Ring. *J. Am. Chem. Soc.* **1987**, *109*, 6878–6880.

(62) Noviandri, I.; Brown, K. N.; Fleming, D. S.; Gulyas, P. T.; Lay, P. A.; Masters, A. F.; Phillips, L. The Decamethylferrocenium/Decamethylferrocene Redox Couple: A Superior Redox Standard to the Ferrocenium/Ferrocene Redox Couple for Studying

Solvent Effects on the Thermodynamics of Electron Transfer. *J. Phys. Chem. B* **1999**, *103* (32), 6713–6722.

(63) Astruc, D. Why Is Ferrocene so Exceptional? *Eur. J. Inorg. Chem.* **2016**, *2017* (1), 6–29.

(64) Long, N. J. *Metallocenes: Introduction to Sandwich Complexes*; Wiley-Blackwell, 1997.